ORNL/TM-2024/3287

Methodological Guidelines for Industry Focusing on Characterization Procedures to Assess the Risk of Irradiation Degradation of Concrete in the Biological Shield

Elena Tajuelo Rodriguez

February 2024

OAK RIDGE National Laboratory

ORNL IS MANAGED BY UT-BATTELLE LLC FOR THE US DEPARTMENT OF ENERGY

ORNL/TM-2024/3287

Light Water Reactor Sustainability Program
M2LW-23OR0403035

Nuclear Energy and Fuel Cycle Division

METHODOLOGICAL GUIDELINE FOR INDUSTRY FOCUSING ON CHARACTERIZATION PROCEDURES TO ASSESS THE RISK OF IRRADIATION DEGRADATION OF CONCRETE IN THE BIOLOGICAL SHIELD

Elena Tajuelo Rodriguez

February 2024

Prepared by
OAK RIDGE NATIONAL LABORATORY
Oak Ridge, TN 37831
managed by
UT-BATTELLE, LLC
for the
US DEPARTMENT OF ENERGY
under contract DE-AC05-00OR22725

CONTENTS

LIST OF FIGURES

LIST OF TABLES

ABBREVIATIONS

AI	artificial intelligence
DOE	US Department of Energy
CNWG	Civil Nuclear Working Group
EMDA	Expanded Materials Degradation Assessment
ICIC	International Committee on Irradiated Concrete
IMAC	Irradiated Minerals, Aggregate and Concrete
JCAMP	Japan Concrete Aging Management Program
LWR	light-water reactor
LWRS	Light Water Reactor Sustainability
MOSAIC	microstructure oriented scientific analysis of irradiated concrete
NCT	neutron computerized tomography
NPP	nuclear power plant
NRC	US Nuclear Regulatory commission
ORNL	Oak Ridge National Laboratory
QEMSCAN	quantitative evaluation of minerals by scanning electron microscopy
RIVE	radiation-induced volumetric expansion
SEM	scanning electron microscopy
SEM-BSE	scanning electron microscopy backscattered electron
SEM-EDS	scanning electron microscopy energy-dispersive x-ray spectroscopy
SONGS	San Onofre Nuclear Generating Station
USAXS	ultrasmall-angle x-ray scattering
XCT	x-ray computed tomography
XRD	x-ray diffraction
XRF	x-ray fluorescence

EXECUTIVE SUMMARY

The extended operation of the US Fleet of light-water reactors (LWRs) to at least 80 years, supported by second license renewals, has posed many questions regarding the effects of irradiation on nuclear power plant (NPP) components. The concrete biological shield (CBS) is expected to be affected by irradiation over long-term operation, given its proximity to the reactor pressure vessel.

In the past decade, the DOE Light Water Reactor Sustainability Program has dedicated some of its resources to investigate the effects of both gamma and neutron radiation on the CBS from experimental and theoretical perspectives. Knowledge has been generated not only by the outcomes of the program, but also by the collaboration with the international research community through the International Committee on Irradiated Concrete (ICIC) and the US–Japan Civil Nuclear Working Group (CNWG)—and by other research efforts funded by the US Nuclear Regulatory Commission (NRC).

This report summarizes the experimental methods that have been used by the irradiated concrete research community to understand the effects of neutrons on aggregates over the past decade. It is structured so that industry can use it as a guiding methodology to estimate the irradiation damage of their unique concrete formulation over extended operation. Two case scenarios are presented:

- Techniques that can be used if access to unirradiated concrete cores from an NPP is possible.

- Techniques that can be employed if access to irradiated aggregates in test reactors is possible.

Limitations on some of the techniques, such as the analysis of microscopy images to obtain crack volume, are discussed, as well as a potential alternative that would mitigate the issues inherent to a 2D technique.

Gaps in knowledge around irradiated concrete research areas are also discussed, such as the lack of understanding of neutron flux effects, gamma and neutron effects on the cement paste, and in-situ creep during irradiation.

The importance of harvesting materials subjected to in-service conditions is also discussed and justified in this report.

ACKNOWLEDGMENTS

This research was sponsored by the US Department of Energy (DOE) Office of Nuclear Energy's Light Water Reactor Sustainability program under contract DE-AC05-00OR22725 with UT Battelle LLC/Oak Ridge National Laboratory (ORNL).

1. INTRODUCTION

1.1 MOTIVATION

The increasing electrical demand in the United States, the power costs, and anthropogenic climate change have made it clear that nuclear energy is a critical component to meeting energy needs. The US Nuclear Regulatory Commission (NRC) has initiated planning and has begun granting several second license renewals to utilities that operate the US fleet of light-water reactors (LWRs). A panel of experts from the NRC, industry, academia, and government entities examined several aspects that needed to be investigated to ensure that plants could remain in operation for the proposed extended period of 80 years associated with second license renewals. These aspects were discussed in the Expanded Materials Degradation Assessment (EMDA) report [1] published in 2014. The effect of irradiation on plant components, including the concrete biological shield (CBS) that surrounds reactor pressure vessels, was considered one of the areas requiring attention—mainly due to a lack of data, knowledge, and understanding of the phenomena governing possible damage.

Since the EMDA was developed, a wealth of knowledge has been created on the effects of irradiation on concrete and its components. Research at Oak Ridge National Laboratory (ORNL) has focused on this topic by compiling and analyzing data on the expansion of minerals and irradiated rocks in the Irradiated Minerals, Aggregate and Concrete (IMAC) database [2], by characterizing samples irradiated in test reactors and harvested from unirradiated parts of a nuclear power plant (NPP) with advanced techniques, and by developing physics-based irradiation damage models. Progress in this area was also made possible by interactions and the exchange of samples and information through the International Committee on Irradiated Concrete (ICIC), the US–Japan Civil Nuclear Working Group (CNWG) and leveraging resources from the NRC to characterize unirradiated concrete cores of San Onofre Nuclear Generating Station (SONGS).

This report summarizes the state-of-the-art methods used to characterize irradiation damage on concrete components to equip industry with guidelines that they could apply to characterize and estimate the irradiation damage in their plant concrete formulation at extended operation.

Substantial effort has been made in characterizing the effects of neutron irradiation on aggregates (rocks embedded in concrete). Two case studies are presented in this report:

1. The possibility to obtain an aggregate sample from a concrete core in an unirradiated area of an NPP.
2. Access to aggregates exposed to relevant neutron doses over extended operation that have been irradiated in test reactors at accelerated conditions.

The limitations of some of the methods, such as image analysis of scanning electron microscopy backscattered electron (SEM-BSE) images for crack volume quantification, are discussed. Alternatives are proposed to address the inherent difficulties and complications of this 2D-based method.

Gaps in knowledge due to environmental factors, such as the effects of temperature and relative humidity on irradiation damage of concrete, as well as the effects of neutron flux are also considered and discussed.

2. CHARACTERIZATION OF EFFECTS OF NEUTRONS ON AGGREGATES

2.1 CASE 1: POSSIBILITY TO OBTAIN A CONCRETE CORE FROM AN UNIRRADIATED PART OF A NUCLEAR PLANT STRUCTURE

2.1.1 Characterization of Aggregate Mineralogy

It has been demonstrated that aggregate mineralogy plays an important role in damage caused by neutron irradiation. Minerals amorphize upon neutron exposure, and this amorphization is accompanied by radiation-induced volumetric expansion (RIVE) [3]. RIVE is much more significant for silicates than for carbonates, and thus concrete expansion depends on the mineral's composition [4]. In the case of silicates, RIVE depends on the silicate polymerization, the relative number of Si–O bonds per unit cell, and the relative bonding energy of the unit cell [4]. There is also a dependency on the bonds' nature because minerals with covalent bonds present more RIVE than do those with ionic ones [4]. Among silicates, quartz is most susceptible to irradiation, experiencing a maximum RIVE of ~18% [4].

Quantifying the mineral phases in an unirradiated aggregate rock is a fundamental step toward estimating its irradiation damage. Several methods to the mineralogy are discussed in this section, as well as how to use the input from these methods to estimate damage and expansion using empirical and physics-based models.

2.1.1.1 Petrography

Purpose: Qualitative identification of minerals and quantitative analysis of grain size.

Sample preparation: Thin section of approximately 20–30 μm of an aggregate mounted on a glass slide with epoxy.

Petrography is a method used in traditional geology, geochemistry, and geoscience for mineral identification. When exposed to plain polarized light and cross-polarized light, minerals display specific colors (birefringence property) that can change when their axis is rotated. Different crystallographic orientations in different grains will give rise to differences in gray scale and color that a petrographic expert will be familiar with. Minerals can be identified using the colors and differences in gray scale. Nevertheless, identifying minerals from petrography can be complex even for an experienced petrographer, and it is an operator dependent process, which justifies the need for other quantitative methods to be develop. An example can be found in Figure 1.

The grain sizes of an aggregate or rock can be analyzed by using image analysis methods such as the watershed algorithm. A detailed example taken from Cheniour et al. [5] is explained here. Before using the watershed algorithm, a combination of binary thresholding and Otsu's thresholding [6] was applied to determine the best threshold value. The next step was generating the markers for the watershed function as local maxima of the distance to the background. This was done by determining the Euclidean distance from all non-zero pixels to the nearest zero pixel or background pixel. The maximum distance was 10 pixels. Then the local maxima map was labeled with a 3 × 3 array that defined feature connections. The result of this process is shown in Figure 2, in which the detected grain boundaries are marked by green lines. Only the particles with detectable grayscale differences are counted in the particle size distribution. Although the method does not detect all grains visible to the naked eye, the number of detected particles is higher than would be detected using the ASTM E1383 method based on manual counts. The resulting grain size distributions are shown in Figure 3.

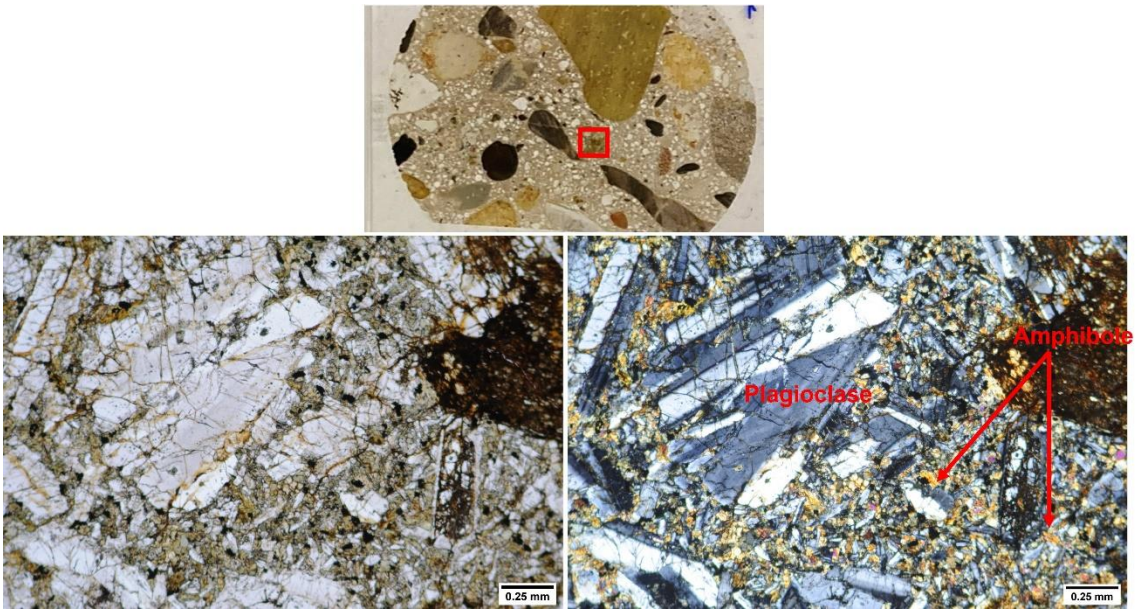

Figure 1. Thin section (top) and petrographic images with uncrossed (left) and crossed polarizers (right) from an aggregate in a core of concrete harvested from SONGS. Taken from [7].

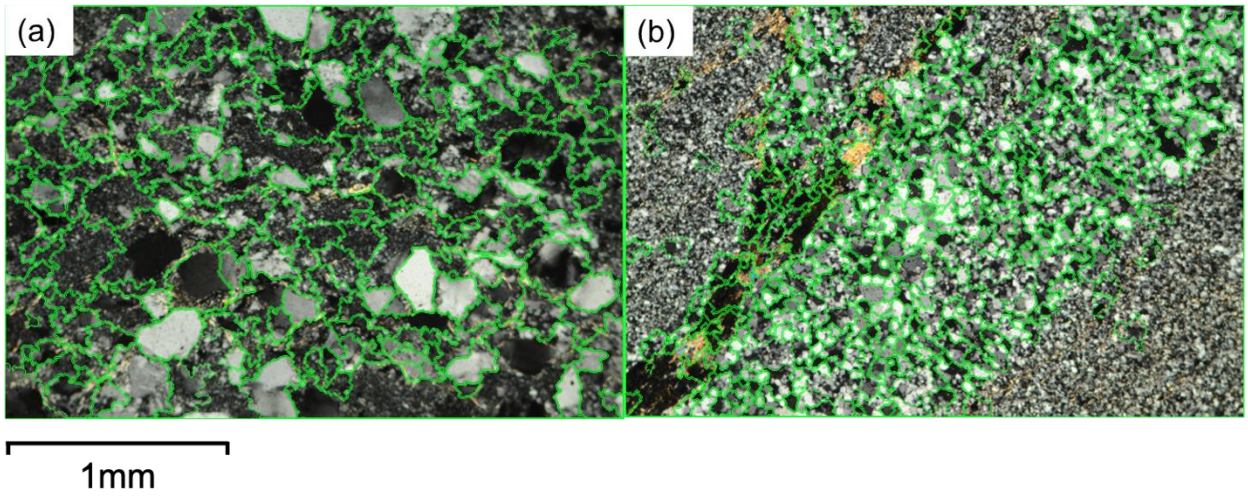

Figure 2. Segmented images of two aggregates using the watershed algorithm: (a) sandstone and (b) meta-chert. Reproduced from Cheniour et al. [5].

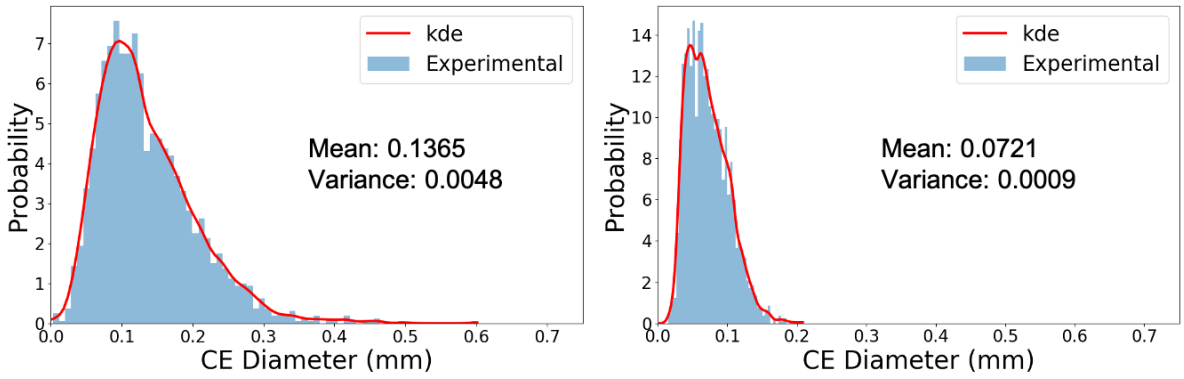

Figure 3. Grain size distributions resulting from the segmentation in Figure 2 for a sandstone (left) and a meta-chert (right) sample. The fitted kernel density distributions are shown in red (kde). Reproduced from Cheniour et al. [5].

2.1.1.2 X-Ray Diffraction with Rietveld Refinement

Purpose: Obtain weight percentages of minerals.

Sample preparation: Grind to fine powder on the order of micron-size particles.

Diffraction patterns depend on crystal structures and are, therefore, a signature of a mineral phase. Various software such as HighScore Plus, TOPAS, FullProff, or GSAS coupled with diffraction pattern databases can be used to perform quantitative analysis to obtain percentages of mineral phases in a sample. For more accurate quantitative results, a standard sample is usually mixed with the specimen to analyze at a known weight fraction. A satisfactory refinement should yield a percentage for the standard sample that is reasonably close to the chosen weight fraction. The results in weight percent of phases can be converted to a volume fraction using the mineral's densities. An example of using Rietveld refinement to obtain the mineral weight percent for different aggregates is found in Maruyama et al. [8].

2.1.1.3 Scanning Electron Microscopy and Energy-Dispersive Spectroscopy (SEM-EDS) with QEMSCAN

Purpose: Quantitative mineral phase analysis via mapping.

Sample preparation: Either thin section mounted on a glass slide or finely polished sample mounted on epoxy or conductive epoxy.

QEMSCAN (FEI) is a software that has been trained by artificial intelligence (AI) with thousands of standards to identify mineral phases. If consecutive maps of several mm^2 are conducted on the surface of an aggregate, then an average composition in phase weight percent can be obtained.

Examples on the use of this software to analyze thin sections of aggregates can be found in Le Pape et al. [7] and in Figure 4.

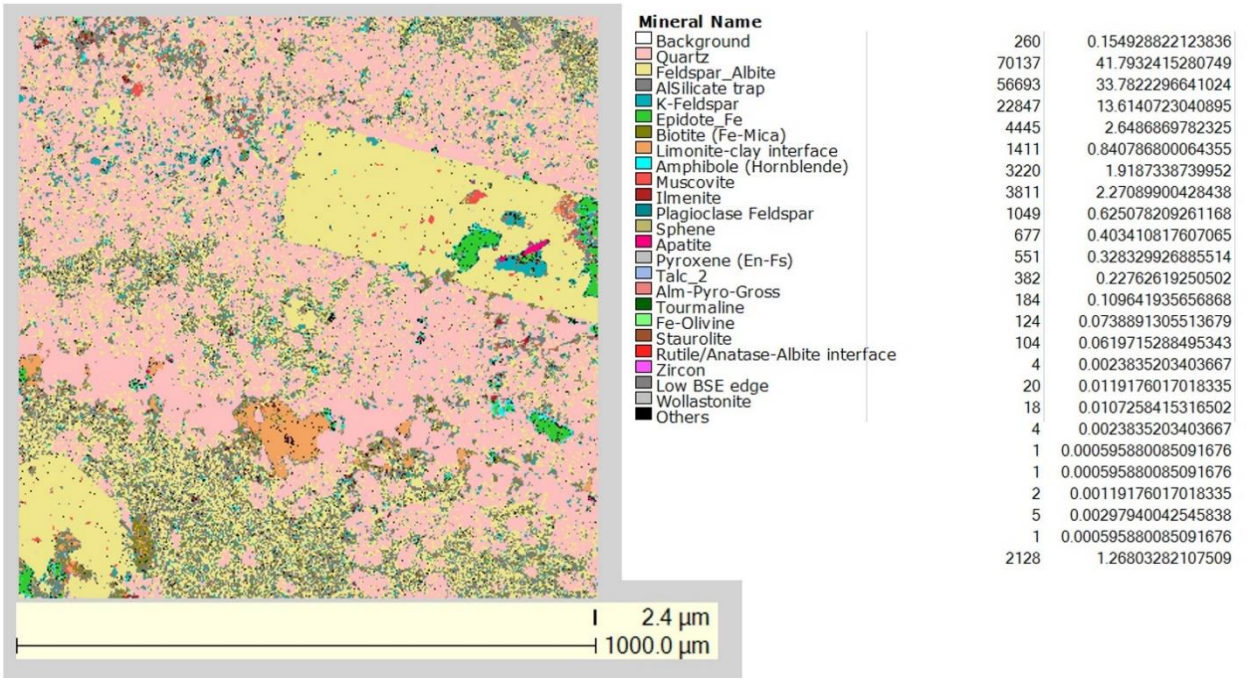

Figure 4. QEMSCAN map from a volcanic aggregate from SONGS concrete. The color legend indicates the mineral phases present, the following column provides the internal QEMSCAN reference for each mineral, and the right-most column shows the percentage of each phase [7].

2.1.1.4 Mapping Informed by X-Ray Fluorescence, SEM-EDS, XRD-Rietveld, and Petrography

Purpose: Obtain a mineral phase map informed by grain size distribution.

Sample preparation: Fine polished surface embedded in epoxy or conductive epoxy for x-ray fluorescence (XRF) and SEM. (For XRD-Rietveld and petrography, see previous sections.)

A method to combine XRF maps and EDS maps for chemical composition, XRD-Rietveld for phase volume fraction, and petrography for grain size distribution to recreate mineral phase maps for aggregates was developed at ORNL [5, 9]. Details are explained in what follows.

The method consists of mapping an area in an aggregate using XRF to identify elements present; however, sodium and lighter elements cannot be accurately detected by XRF due to limitations of the technique. Moreover, because sodium is present in silicate minerals such as albite, pyroxenes, micas, and amphiboles that are common in felsic igneous rocks (e.g., granite), detecting this element is crucial in reconstructing mineral phase maps. To compensate for this limitation, SEM-EDS maps can be created in the same area for the same elements detected by XRF to enable the detection of sodium. The EDS elemental maps are then resized to the same pixel size of the XRF using bilinear interpolation and smoothed with an averaging filter. Correlations between sodium and other elements are established. The strongest element–element correlation is then chosen to reconstruct the sodium map. To reconstruct the sodium map over the entire aggregate, a linear regression analysis is performed on the correlation. Details on the full process for reconstruction of the sodium map can be found in Li et al. [9].

The next step includes the creation of particle maps based on elemental concentrations given by the XRF maps. This can be done using the Microstructure Oriented Scientific Analysis of Irradiated Concrete (MOSAIC) software developed at ORNL [10]. The software counts with a tool that scans the elemental concentrations and defines particles based on the proximity of the concentration values. The element concentration for each particle is the average concentration of all pixels included in the particle, plus the boundary pixels.

The following step is the phase assignment using an empirical approach that consists of three substeps:

1. Identification of elements that correlate with the presence or absence of the minerals of interest.
2. Estimation of the likelihood of the presence of a given mineral based on its chemical composition and the concentration of elements determined by XRF.
3. Assignment of phases to approximate the volume fractions given by XRD with Rietveld refinement.

When the phases are assigned, the grain size distribution obtained by petrography is used to impose a grain structure in the minerals. This step requires adapting parameters, such as the neighborhood size in MOSAIC's particle map generation, to search for concentration gradients that match a similar particle size distribution to that obtained by petrography.

An example of phase maps obtained with these methods for a Japanese meta-chert and four different Japanese sandstones is depicted in Figure 5. These types of maps can be input into MOSAIC to estimate RIVE and damage for irradiated aggregates. Details on how to perform MOSAIC simulations using these maps as input can be found in Cheniour et al. [5].

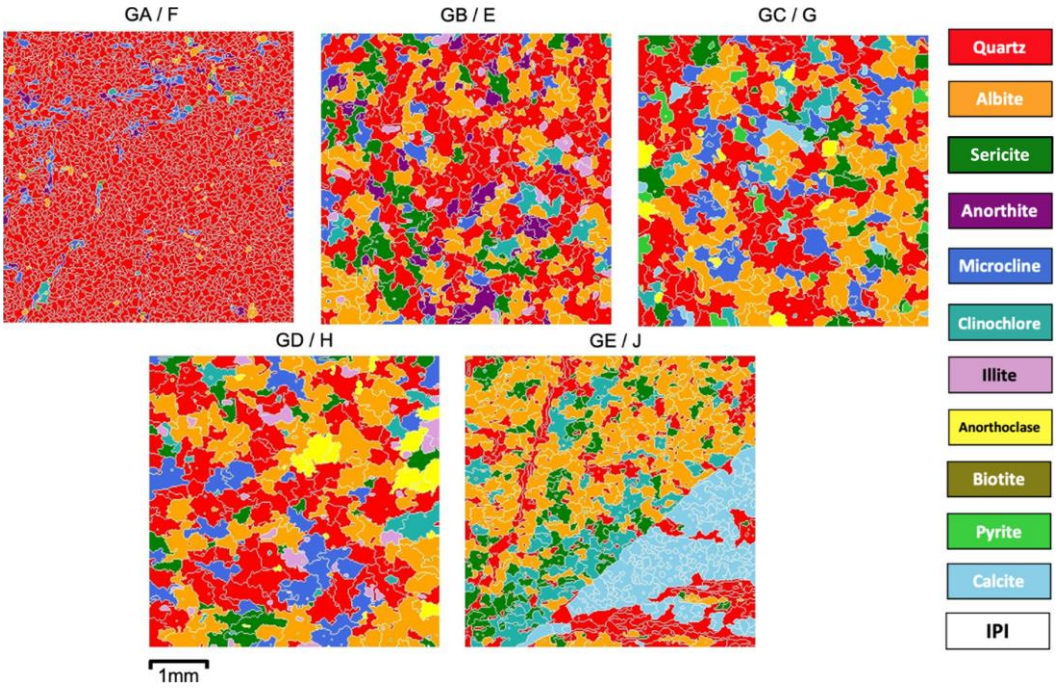

Figure 5. Mineral phase maps of a meta-chert aggregate (GA/F), and four sandstone aggregates (GB/E, GC/G, GD/H and GE/J. Reproduced from Cheniour et al. [5].

2.1.2 Expansion Estimation Based on Mineralogy Input Using the IMAC Database

Information on the weight percent of mineral phases obtained from XRD with Rietveld refinement or SEM-QEMSCAN mapping can be used to estimate the volumetric expansion of an aggregate/rock by using information on expansion of minerals present in the IMAC database. Knowledge of an approximate gradient of neutron fluence expected in the inner surface of the CBS considering the operation period is necessary for damage assessment; additionally, an approximate temperature gradient in the CBS is needed to extract the relevant expansion data from the database.

The best-estimate expansions can be calculated using RIVE models derived from extensive data included in the IMAC database [2, 4].

An example taken from Le Pape et al. [7] is given below for several aggregates extracted from a concrete core of the non-irradiated structure of SONGS:

The compositions of the aggregates given by XRD with Rietveld refinement are as follows:

1. Agg. 1: Quartz (37%), microcline intermediate (36%), and albite (27%)
2. Agg. 2: Quartz (52%), albite (34%), and microcline intermediate (14%)
3. Agg. 3: Quartz (72%), albite calcian (17.5%) and Biotite-1M (10.9%)
4. Agg. 4: Quartz (92%), Muscovite 2M-1 sodian (4.3%) and albite calcian (3.3%)
5. Agg. 5: Quartz (48%), albite calcian (47%), clinochlore ferroan (4.4%)

The approximate fluence and temperature intervals are as follows:

- The estimated fluence interval received by the CBS at end of operation is 1.9–3.57 × 10^{19} n/cm^2 (E > 0.1 MeV or 10 keV)
- The estimated temperature interval is 40–65°C

Given these compositions, the minerals of interest are quartz, feldspars, and mica. According to the models in Le Pape et al. [4], the RIVEs associated with these minerals are those presented in Table 1.

Table 1. Estimated RIVES of different minerals according to empirical models in the IMAC database.

	Fluence × 10^{19} n/cm^2 (E > 10 keV)	1.9		3.57	
RIVE (%)	Temperature (ºC)	40	65	40	65
	Quartz	1.8	0.7	4.2	1.7
	Feldspar	< 0.01	< 0.01	< 0.01	< 0.01
	Mica	0.4	0.4	0.7	0.7

An increase in temperature has an annealing effect on expansion; therefore, the estimate at 40°C is considered a lower bound value, whereas the estimate at 65°C is considered an upper bound value.

The estimated RIVEs for the aggregates were calculated using the percentages of minerals in each aggregate; these values are shown in Table 2. This method does not account for the creation of cracking caused by mismatched expansion between adjacent minerals.

Table 2. Estimated RIVE values of different aggregates based on their mineralogy.

RIVE (%)	Fluence × 10^{19} n/cm^2 (E > 10 keV)	1.9		3.57	
	Agg. 1	0.67	0.27	1.56	0.64
	Agg. 2	0.94	0.37	2.19	0.89
	Agg. 3	1.35	0.56	3.12	1.32
	Agg. 4	1.67	0.66	3.89	1.59
	Agg. 5	0.89	0.36	2.05	0.85

2.2 CASE 2: POSSIBILITY OF IRRADIATED AGGREGATES IN TEST REACTORS AND COMPARISON OF PROPERTIES WITH UNIRRADIATED SPECIMENS

2.2.1 Characterization of Expansion of Irradiated Aggregates

Several methods to measure the post-irradiation expansion including cracks, pores, and the expansion of the crystallographic cells of the minerals in aggregates are discussed in this section.

2.2.2 Dimensional Measurements (Expansion Due to Cracking and Expansion of Mineral Cell Volume)

Purpose: Measure the volume expansion of irradiated aggregate.

Sample preparation: None.

The overall expansion of aggregates after irradiation with neutrons is caused by two phenomena: the expansion of the minerals' unit cell volume and the opening of cracks. The easiest way to calibrate this overall expansion is to compare sample dimensions before and after irradiation. Recommended methods typically used include the use of calipers, touch probes or laser-based dimensional measurements. A schematic of locations for dimensional measurements taken for irradiated Japanese aggregates is shown in Figure 6. Example applications can be found in the work of Maruyama et al. [8, 11].

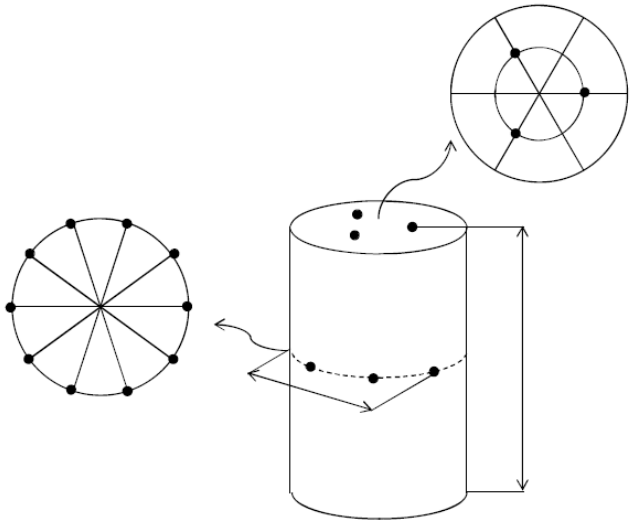

Figure 6. Locations for dimension measurements of irradiated aggregates (5 diameters and three heights). Reproduced from [11].

2.2.3 Crack Volume (X-Ray Computed Tomography, SEM, Helium Pycnometry)

Purpose: Estimate the crack volume on irradiated aggregate.

Sample preparation: None for x-ray computed tomography (XCT) or pycnometry. Fine polish and epoxy mount for SEM.

Crack volume can be estimated by image analysis of XCT-based measurements or SEM-BSE image analysis shown in Figure 7. An example explaining a method for quantifying cracks based on SEM images is detailed in Maruyama et al. [11]. The method is based on a Python code and consists of the following steps:

- Contrast correction (thresholding)
- Classification of each pixel based on grayness level: dark, dark gray, light gray, and white
- Segmentation
- Skeletonization
- Statistical evaluation

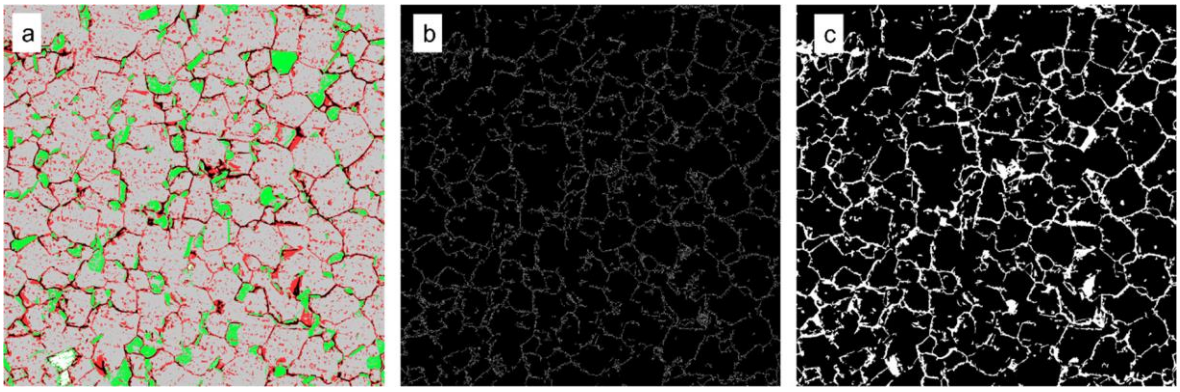

Figure 7. Analysis of SEM-BSE images of an irradiated aggregate showing thresholding (a), skeletonization (b), and resulting detected crack patter (c). Reproduced from Maruyama et al. [11].

The volume of small aggregate samples can be estimated by helium pycnometry. This process of gas-based measurement consists of collecting the volume of gas that can fill a sample carrier and the volume of gas that fills the sample carrier with the sample contained in it. The difference between those two gas volumes is the sample volume. Helium gas can penetrate cracks that are open to the sample surface and can serve to estimate irradiation-induced solid density changes (by measuring weight) and irradiation-induced crack volume. Examples of the use of helium pycnometry for irradiated aggregates are discussed in Maruyama et al. and Tajuelo Rodriguez et al. [11, 12].

Closed porosity cannot be accessed by the gas, but a method discussed in Section 2.2.6. can yield an estimation for both open and closed pores from the nanoscale to the microscale. Closed pores can also be measured at the microscale with x-ray or neutron computed tomography (XCT or NCT), given that its ultimate resolution lies in the micron range.

2.2.4 Expansion of Mineral Unit Cell Volume (XRD)

Purpose: Measure expansion of the unit cell of minerals caused by neutrons.

Sample preparation: Grind to fine powder on the order of micron-size particles.

Expansion caused by amorphization of the crystalline structure of the minerals can be measured by XRD combined with Rietveld refinement. The atomic distances or d-spacings in XRD can be calculated by the following equation:

$$d = \frac{n\lambda}{2\,sin\theta}\,, \qquad (1)$$

where n is an integer, λ is the wavelength of the x-rays, and θ is the x-ray incidence angle. Patterns are usually displayed as arbitrary intensity vs. 2θ or vs. d-spacing.

As the minerals' unit cells deform and expand with neutron bombardment, the Bragg peaks shift to lower 2θ angles (larger d-spacings). By using Rietveld refinement, the dimensions of the unit cell can be fitted and calculated from XRD patterns to estimate the cell volume expansion. This was used by Maruyama et al. [11] to calculate the unit cell expansion of quartz in a Japanese tuff or meta chert aggregate.

2.2.5 Comparison of Pycnometry, Unit Cell, and SEM Image Analysis for Expansion of Aggregates and Its Limitations

RIVE values of quartz estimated by dimensional change, XRD unit cell, and pycnometry measurements were compared for a Japanese tuff or meta-chert irradiated to different neutron fluences, as shown in Figure 8. The results of helium pycnometry and XRD cell volume expansions are equivalent when considering the percentage of quartz in the sample (85%) and multiplying the XRD volume expansion of the unit cell by 0.85. The difference between the expansion measured by dimensional changes and the expansion measured by pycnometry must be accounted for by the volume of crack opening. This volume can be calculated by image analysis of SEM-BSE images with the method described in Section 2.2.3. However, the percentage of crack volume obtained by image analysis was much higher than the difference between volumetric expansion calculated by dimensional and helium pycnometry measurements. This discrepancy might have occurred because SEM imaging was performed in a very localized area of the aggregate that must not be representative of the bulk because additional cracks could have appeared due to sample preparation and polishing, and/or due to errors that could be associated with extrapolation of 2D crack areas to 3D crack volume.

A better method to establish the crack volume in 3D could be to analyze XCT images with micron resolution, since it does not require sample preparation and gives a 3D reconstruction of the volume. This will be the subject of a further milestone report based on analysis of synchrotron-based tomography images of Japanese irradiated aggregates. This future milestone is part of the Irradiated Concrete work package for fiscal year 2024.

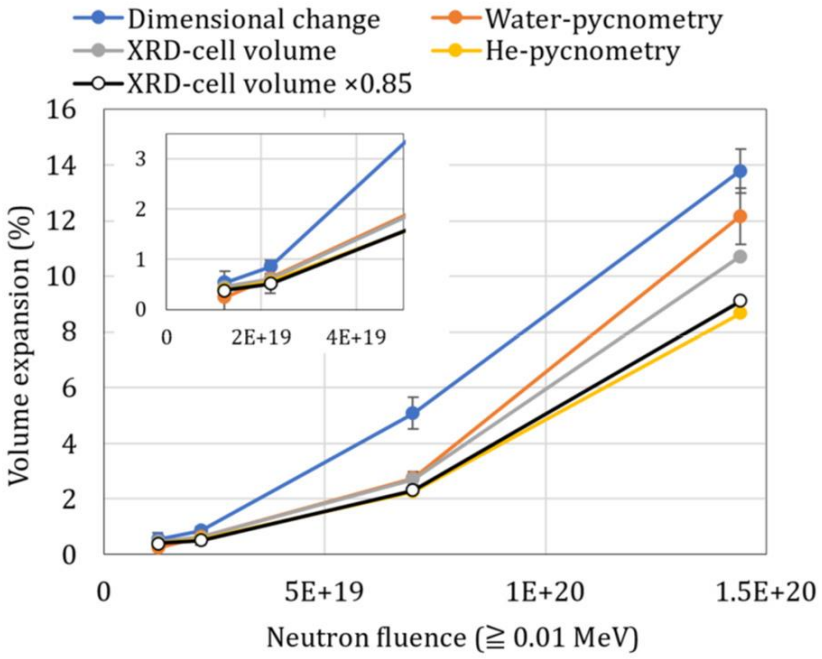

Figure 8. Comparison between RIVE calculated by dimensional changes, XRD cell volume changes, and two types of pycnometry (helium and water) for a Japanese tuff or meta-chert aggregate.
Reproduced from Maruyama et al. [11].

2.2.6 Nanoporosity (Ultrasmall-Angle X-Ray Scattering)

Purpose: Estimate cumulative porosity for pores in the range of 100 nm and 2 µm.

Sample preparation: Polish thin sections to a thickness of approximately 20 µm (epoxied to glass slides).

Nanopores and submicron pores can be challenging to resolve with imaging methods. Taking advantage of the dimensions that x-rays can explore—given their wavelengths—makes it possible to use techniques such as synchrotron-based ultrasmall-angle x-ray scattering (USAXS) to access the porosity at those length scales.

Scattering curves for rocks are the result of scattering contrast between air in pores and minerals. Models to fit scattering curves to obtain porosity distributions have been developed in the Irena software package [13] for Igor Pro. Several options are available to derive the porosity distributions with methods such as the total non-negative least squares or maximum entropy. The latter method was applied to a series of Japanese aggregates of different mineralogy (a tuff or meta-chert, four sandstones, and a limestone) irradiated to different neutron doses and their unirradiated counterparts [12]. Porosity distribution curves provide interesting information but can be misleading because peaks that appear large at small pore sizes do not contribute significantly to the overall pore volume. An easier interpretation of these curves can be done by integrating the area below them. The integral yields the cumulative pore volume. This can be compared directly for the same rock irradiated to different neutron doses and between rocks of different mineralogy (Figure 9).

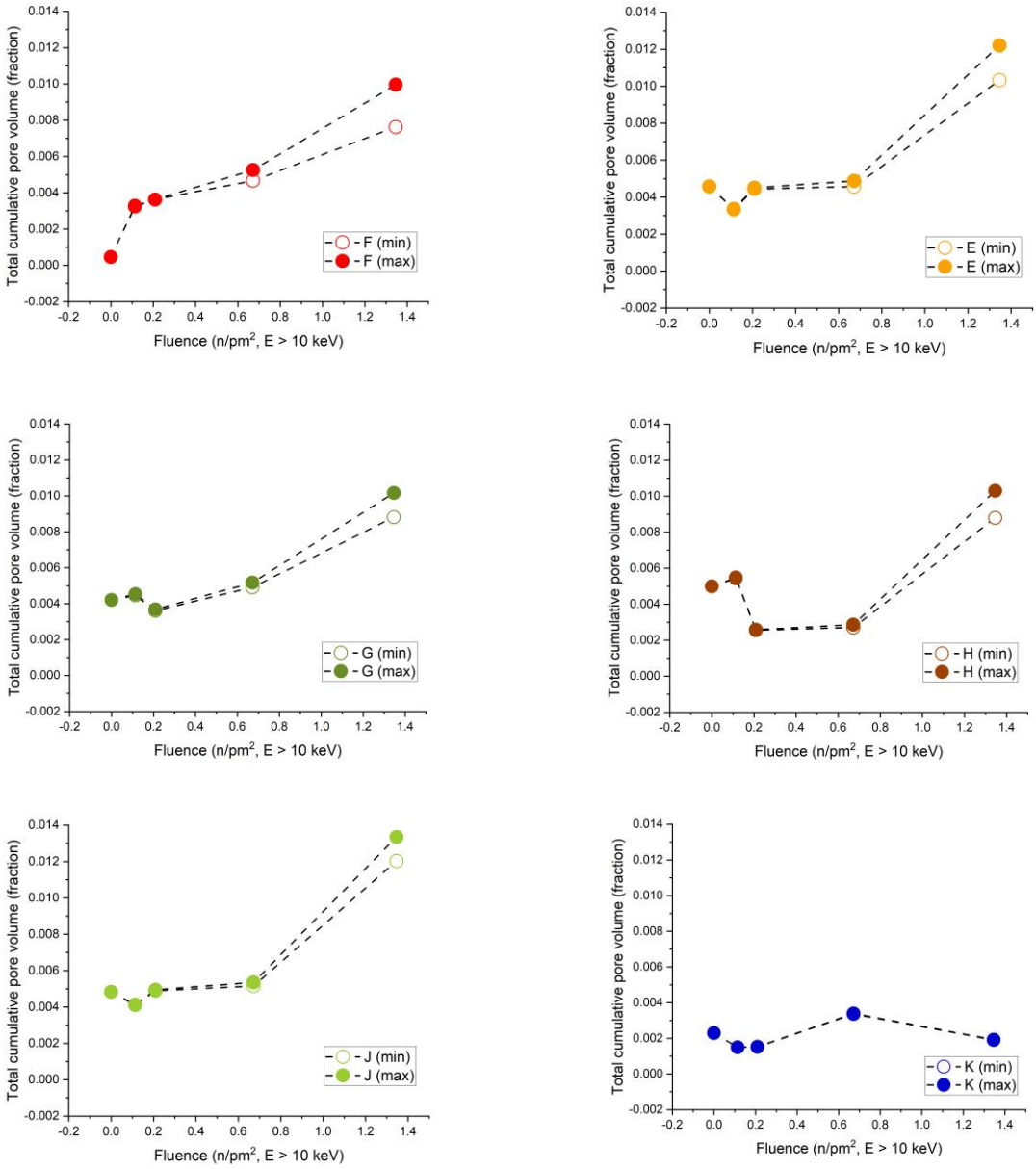

Figure 9. Total cumulative porosity for pores of sizes between 100 nm and 2 μm for Japanese aggregates of different mineralogy as a function of neutron fluence. F is a tuff or meta chert, E, F, G, and H are sandstones, and K is a limestone.

2.2.7 Mechanical Properties by Ultrasound Pulse Velocity

Purpose: Measure post-irradiation bulk mechanical properties via ultrasound pulse velocity and local mechanical properties (mini-tension tests) in aggregates.

Sample preparation: None.

Non-destructive evaluation methods are ideal to measure the mechanical properties of irradiated aggregate specimens because no sample preparation is required. The use of both longitudinal and shear waves allows for the estimation of Young's modulus (E), shear modulus (G), and Poisson's ratio (v). The measured wave velocities (v_L and v_S) and an estimate of the density (ρ) are needed to calculate the moduli and Poisson's ratio. They can be calculated with the following expressions:

$$\nu = \frac{V_L^2 - 2V_S^2}{2(V_L^2 - V_S^2)}, \quad (2)$$

$$G = \rho V_S^2 , \quad (3)$$

$$E = 2G(1 + \nu) . \quad (4)$$

In this case, the density measured by directly weighing and obtaining the dimensions of the samples (known as *apparent density*) should be used instead of that obtained through pycnometry. This is because mechanical properties will be the result of interactions of the waves with both solid material and pores. Examples of measurements of the relative Young's moduli of irradiated Japanese aggregates of different mineralogy vs. their RIVE are shown in Figure 10 . More examples of measurements of wave velocities and calculated moduli can be found in Tajuelo Rodriguez et al. [12].

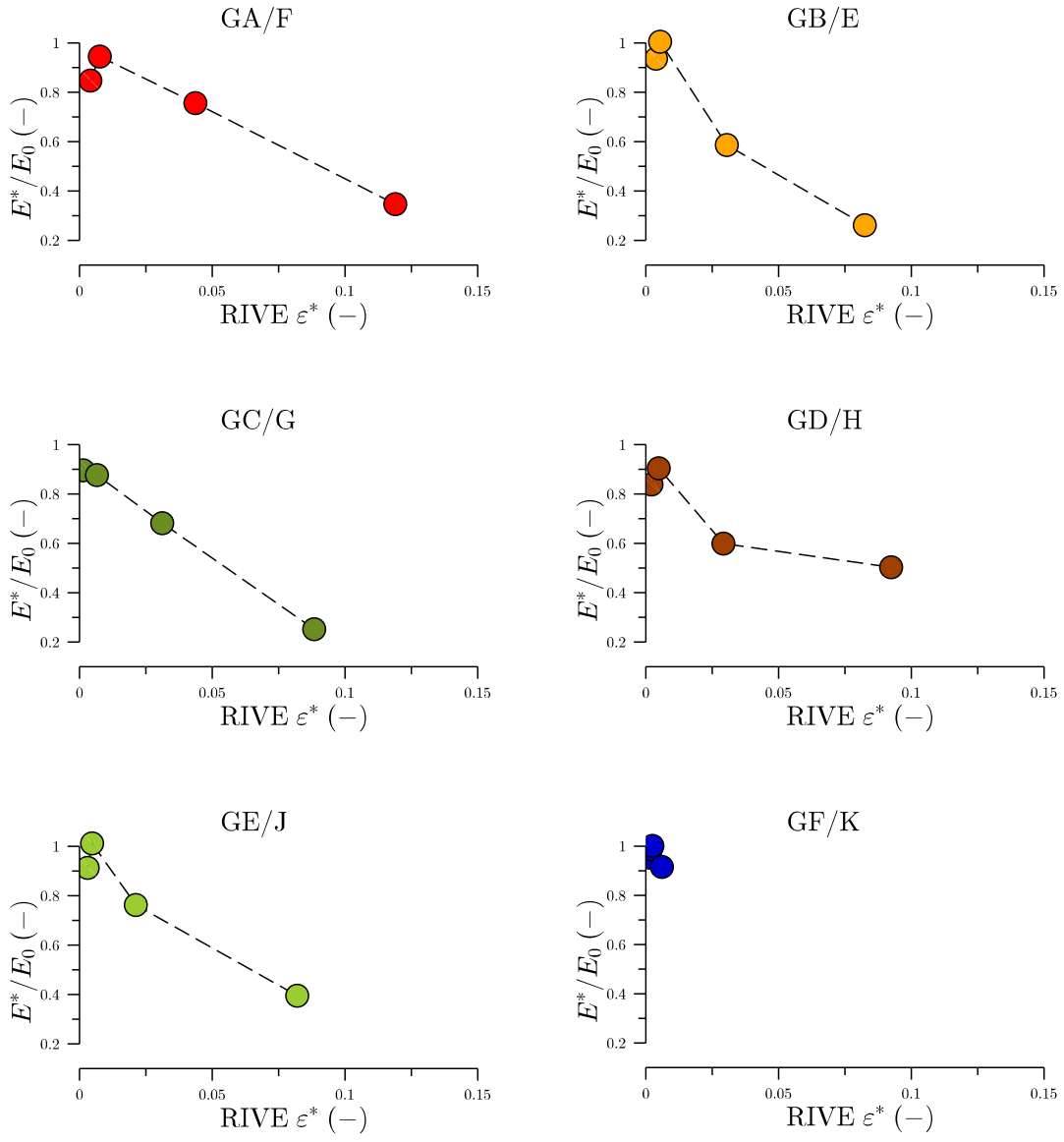

Figure 10. Evolution of relative Young's modulus with RIVE for Japanese aggregates of different mineralogy.
F is a tuff or meta chert, E, F, G, and H are sandstones, and K is a limestone.
Taken from Tajuelo Rodriguez et al. [12].

2.2.8 Mechanical Properties by Macroscopic Compression and Splitting Tensile Strength Tests and Microscopic Tensile Tests

Purpose: Evaluate macroscopic and microscopic mechanical properties of irradiated aggregates.

Sample preparation: Drilling, cutting, and polishing to desired and relevant dimensions per test.

Maekawa et al. [14] conducted several compression and tensile tests for a tuff or meta-chert aggregate. The compressive strength and Young's modulus of the aggregate were measured by macroscopic compression tests. Brazilian tests, or macroscopic splitting tensile strength tests, were used to measure the splitting tensile strength of the aggregates. Local mechanical properties in areas of different grain sizes were tested by microscopic tensile strength tests in which the stress–strain behavior of tiny specimens was investigated. The pre-existing cracks and defects were found to yield a larger compressive than tensile Young's modulus. The macroscopic tensile strength was greater than the local or microscopic tensile strength due to differences in crack development during both kinds of tests. The microscopic tensile tests reflected the local strength due to the grain texture. These mechanical tests can be applied to similar regions of the irradiated aggregate to compare macroscopic and microscopic property changes with irradiation.

3. THE ROLE OF NEUTRON FLUX ON CONCRETE DEGRADATION AND KNOWLEDGE GAPS AROUND IRRADIATED CONCRETE

Most irradiation studies on aggregates are based on samples irradiated in test reactors. The neutron flux in those reactors is orders of magnitude higher than neutron fluxes expected in the CBS during in-service conditions. This suggests that for a given neutron dose, the expansion and damage obtained during test reactor experiments might be larger than those expected under actual operation conditions. This is equivalent to considering acute and prolonged irradiation doses to tissue. The effects of these are well known; acute doses can cause significantly more damage than prolonged small doses in time. The role of relaxation mechanisms and the time the materials are given to recover from neutron and gamma exposure is important and is not well understood.

Other factors such as the impact of gamma rays [15-22] and neutrons [23] on the cement paste are not fully explained at this time because most studies are done post-irradiation and ignore complex dehydration phenomena and creep responses that could be occurring during irradiation cycles. In-situ irradiation creep experiments are scarce [20], and more research in this area is needed to shed light on these phenomena. The role of possible chemical reactions that might be occurring by the combination of irradiation and environmental factors, such as temperature and relative humidity, is also crucially important and is currently unexplored. A recent example of an unexpected result obtained through harvesting samples of the CBS of the Hamaoka power plant reveals the importance of the consideration of chemical reactions on irradiated concrete. It was found that the strength of the cement paste was enhanced by the precipitation of a mineral phase (tobermorite) that occurred due to very particular conditions of temperature and relative humidity coupled with irradiation [24].

All these factors underline the importance of harvesting materials that have been exposed to in-service conditions to verify the hypothesis of damage dependence on flux effects, and how other environmental conditions might impact the integrity and properties of concrete over long-term operation.

4. CONCLUSIONS

This report presents methodological guidelines for industry to assess potential irradiation damage of their concrete formulation over extended operation periods. It describes experimental methods that can be used to characterize the chemical and physical properties of unirradiated and irradiated aggregates. Two case scenarios are envisioned:

- The possibility to obtain unirradiated concrete cores from an NPP.

- The possibility to access aggregates irradiated in test reactors.

Experimental methods used by the international research community to characterize the aggregates are discussed for both scenarios. The first scenario considers methods to analyze the mineralogy of the aggregates and use it as input for empirical models and fast Fourier transform models for the estimation of expansion and irradiation damage. The second scenario considers measurements to compare physical properties of the aggregates pre- and post-irradiation to account for expansion, porosity generation, and crack opening induced by the neutron bombardment.

Limitations on some of the techniques, such as the image analysis of SEM micrographs to obtain crack volume, are discussed. XCT is presented as an alternative technique given that it yields information directly in 3D without any sample preparation.

The lack of understanding of neutron flux effects, gamma and neutron effects on the cement paste, and in-situ creep during irradiation is also discussed, leaning toward the necessity to perform in-situ creep irradiation experiments and to harvest materials from decommissioned NPPs.

REFERENCES

1. Graves, H., et al., *Expanded material degradation assessment (EMDA), Volume 4: Aging of concrete.* Technical Rep. NUREG/CR-7153, ORNL/TM-2011/545, United State Nuclear Regulatory Commission, Rockville, MD, 2014.
2. Le Pape, Y., *IMAC Database v.0.1. - Minerals, Light Water Reactor Sustainability Program*. 2016.
3. Field, K.G., I. Remec, and Y. Le Pape, *Radiation effects in concrete for nuclear power plants–Part I: Quantification of radiation exposure and radiation effects.* Nuclear Engineering and Design, 2015. **282**: p. 126-143.
4. Le Pape, Y., M.H.F. Alsaid, and A.B. Giorla, *Rock-Forming Minerals Radiation-Induced Volumetric Expansion – Revisiting Literature Data.* Journal of Advanced Concrete Technology, 2018. **16**(5): p. 191-209.
5. Cheniour, A., et al., *FFT-based model for irradiated aggregate microstructures in concrete.* Materials and Structures, 2022. **55**(8): p. 214.
6. Otsu, N., *A threshold selection method from gray-level histograms.* IEEE transactions on systems, man, and cybernetics, 1979. **9**(1): p. 62-66.
7. Le Pape, Y., Tajuelo, E., Bran Anleu, P., Brooks, A., Anovitz, L. M., Arpan, A., Sheets, J., Koehler, M., Rother, G., Rosseel, T. M., *Assessment of San Onofre Concrete Susceptibility Against Irradiation Damage, RIL 2022-07*.
8. Maruyama, I., et al., *Development of Soundness Assessment Procedure for Concrete Members Affected by Neutron and Gamma-Ray Irradiation.* Journal of Advanced Concrete Technology, 2017. **15**: p. 440-523.
9. Li, Y., et al., *Microstructural characterization and assessment of mechanical properties of concrete based on combined elemental analysis techniques and Fast-Fourier transform-based simulations.* Construction and Building Materials, 2020. **257**: p. 1195.
10. Torrence, C.E., et al., *MOSAIC: An Effective FFT-based Numerical Method to Assess Aging Properties of Concrete*. Journal of Advanced Concrete Technology, 2021. **19**(2): p. 149-167.
11. Maruyama, I., et al., *Radiation-induced Alteration of Meta-chert.* Journal of Advanced Concrete Technology, 2022. **20**(12): p. 760-776.
12. Tajuelo Rodriguez, E., Arregui-Mena, D., Cheniour, A., Li, Y., Le Pape, Y., Anovitz, L. M., Cheshire, M. C., Weber, J., Cakmak, E., Polavaram, K., Garg, N., *Multi-Technique Characterization of Porosity and Cracks in Pristine and Neutron-Irradiated Aggregates Complemented by Mosaic Simulations*. 2021.
13. Ilavsky, J. and P.R. Jemian, *Irena: tool suite for modeling and analysis of small-angle scattering.* Journal of Applied Crystallography, 2009. **42**: p. 347-353.
14. Maekawa, K., et al., *Microscopic and Macroscopic Physical Properties of Meta-chert.*
15. Baral, A., Tajuelo Rodriguez, E., Hunnicutt, W. A., Le Pape, Y., Rosseel, T., Garg, N., *Ultra-High Gamma Irradiation of Calcium Silicate Hydrates: Evidence of Damage in 1H and 29Si Atomic Environments.* Submitted to Cement and Concrete Research, 2021.
16. Hilloulin, B., M. Robira, and A. Loukili, *Coupling statistical indentation and microscopy to evaluate micromechanical properties of materials: Application to viscoelastic behavior of irradiated mortars.* Cement and Concrete Composites, 2018. **94**: p. 153-165.
17. Hunnicutt, W., et al., *Examination of Gamma-irradiated Calcium Silicate Hydrates. Part II: Mechanical Properties.* Journal of Advanced Concrete Technology, 2020. **18**(10): p. 558-570.
18. Kontani, O., et al. *Evaluation of irradiation effects on concrete structure: Gamma-ray irradiation tests on cement paste*. in *ASME 2013 Power Conference*. 2013. American Society of Mechanical Engineers.
19. Łowińska-Kluge, A. and P. Piszora, *Effect of gamma irradiation on cement composites observed with XRD and SEM methods in the range of radiation dose 0-1409 MGy.* Acta Physica Polonica-Series A General Physics, 2008. **114**(2): p. 399.

20. McDowall, D. *The Effects of Gamma Radiation on the Creep Properties of Concrete*. in *Proceedings of an Information Exchange Meeting on 'Results of Concrete Irradiation Programmes'*. 1971.
21. Tajuelo Rodriguez, E., et al., *Examination of gamma-irradiated calcium silicate hydrates. Part I: Chemical-structural properties.* Journal of the American Ceramic Society, 2020. **103**(1): p. 558-568.
22. Robira, M., et al., *Multi-scale investigation of the effect of γ irradiations on the mechanical properties of cementitious materials.* Construction and Building Materials, 2018. **186**: p. 484-494.
23. Krishnan, N.M.A., et al., *Revealing the Effect of Irradiation on Cement Hydrates: Evidence of a Topological Self-Organization.* ACS Applied Materials & Interfaces, 2017. **9**(37): p. 32377-32385.
24. Maruyama, I., et al., *Long-term use of modern Portland cement concrete: The impact of Al-tobermorite formation.* Materials & Design, 2021. **198**: p. 109297.